

342 yielded significantly lower deposition fluxes. GOM breakthrough may not occur in all cases. For
343 example, if there are temperature drops within the instrument, then GOM will deposit to the
344 walls (Gustin et al., 2013). Because of these issues, the authors conclude it is presently more
345 robust to interpret RM rather than PBM and GOM data separately.

346

347 **3.3 GOM: Biases, interferences, and shedding light on the spatiotemporal variability of**
348 **GOM compounds in air**

349 Based on laboratory and field studies, concentrations of GOM collected on the nylon and
350 cation exchange membranes are higher than those collected by the Tekran® system by 60-
351 1000% (Huang et al., 2014; Huang and Gustin, 2015a; 2015b). Laboratory and field experiments
352 have demonstrated the collection efficiency of KCl-coated denuders varies with environmental
353 conditions (O₃, RH) and Hg(II) compounds present in air. Below we discuss recent laboratory
354 experiments and field studies that have shaped our understanding of the limitations of GOM
355 measurement methods.

356

357 *3.3.1 Ozone and relative humidity interferences*

358 Laboratory experiments have confirmed O₃ interferences for KCl-coated denuders and
359 relative humidity (RH) interferences for both denuders and nylon membranes (Lyman et al.,
360 2010a; McClure et al., 2014; Huang and Gustin, 2015b). Lyman et al. (2010a) found the
361 collection efficiency of HgCl₂ loaded on a KCl denuder was reduced by 3 to 37% when O₃
362 concentrations were 6 to 100 ppbv. Lyman et al. (2010a Open Discussion) proposed reduction
363 was occurring on the denuder wall:



365 Their results also indicated less GOM was recovered as O₃ exposure time increased (10 to 26%
366 removed from loaded denuders for 2.5 minutes, and 29 to 55% for 30 minutes at 30 ppbv).

367 In experiments similar to those performed for O₃, McClure et al (2014) found RH had a
368 similar effect on HgBr₂ loaded on KCl-coated denuders. Huang and Gustin (2015a) permeated
369 HgBr₂ and water vapor into a Tekran® 2357/1130 system in ambient air and found collection
370 efficiencies dropped during the spikes of RH, and the denuder became passivated over time.

371 They found at RH of 21 to 62%:

372 RH= 0.63 GOM loss% + 18.1, r²=0.49, p-value < 0.01. Equation 2.

373 Huang and Gustin (2015a) found a greater impact of relative humidity than O₃.

374

375 *3.2.2 Variability of RM composition and concentrations*

376 Here we use comparisons of data collected with a variety of sampling methods to better
377 understand atmospheric Hg concentrations, and how measurement discrepancies vary with
378 environmental setting (e.g., RH and O₃) and Hg(II) compounds present in the ambient
379 atmosphere. This includes data collected as part of a large study in Florida (Peterson et al., 2012;
380 Gustin et al., 2012), the RAMIX field campaign (Gustin et al., 2013), recent comparison of KCl-
381 coated denuder data with the UNR active system (Huang et al., 2013; 2015), and laboratory
382 testing (Huang et al., 2013; Huang and Gustin, 2015a and b). For a historical review of additional
383 literature see the supplemental information in Gustin et al., 2013, Huang et al., 2014, and SI this
384 paper.

385 Peterson et al. (2012) compared passive samplers and Tekran® data from three sites in
386 Florida. The region has high Hg wet deposition, but low GOM concentrations (on average 2-8 pg
387 m⁻³ as measured by the Tekran® system). In general, the Aerohead or dry deposition sampling

388 system (described above), showed higher deposition for GOM than that calculated using KCl-
389 coated denuder concentrations and a dry deposition model. Based on passive sampler uptake and
390 calculated deposition velocities, Peterson et al. (2012) suggested the difference could be
391 explained by the presence of different GOM compounds in the air (see SI for additional detail).
392 Examining the data across all seasons, using three Hg measurement methods, criteria pollutants,
393 and meteorology, Gustin et al. (2012) concluded there were different GOM compounds in air
394 that were derived from different primary sources, sources producing different oxidants, and
395 variation across season.

396 Data from the RAMIX experiment also indicated the KCl-denuder measurements were
397 biased low through spikes of GOM ($HgBr_2$) into a manifold. Ambient air RM concentrations
398 measured by the DOGHS were higher than those measured by the Tekran® system and this
399 instrument recovered 66% of the $HgBr_2$ spike during the Reno Atmospheric Mercury
400 Intercomparison eXperiment (RAMIX) (Gustin et al., 2013). The experiment also indicated RH
401 caused the denuders to become passivated over time (Gustin et al., 2013). Spike recoveries of
402 $HgBr_2$ by KCl-coated denuders were 2-to-5 times lower than that measured by the DOGHS, with
403 mean values for spikes ranging from 17 to 23% recovery. Replicate nylon membranes collected
404 30 to 50% more RM than the Tekran® system in ambient air. For a concise summary of the
405 results of the RAMIX DOHGS versus Tekran® data, and an explanation for a component of the
406 atmospheric chemistry occurring see the SI.

407 Figure 1 and Table 2 show correlations between specific GOM compounds
408 concentrations measured by the nylon and cation exchange membranes versus the KCl-coated
409 denuder in the Tekran® system (see Huang et al. (2013) for detail on the experimental setup).
410 These data demonstrate different compounds have different collection efficiencies by the

411 denuder. Figure 1 shows the nylon membrane has equal efficiency for all Hg(II) compounds
412 tested, and the cation exchange membrane quantitatively collects the Hg(II) compounds
413 permeated. The collection efficiency of the cation exchange membrane relative to the KCl-
414 coated denuder in a Tekran® 1130 is HgBr₂ (1.6)>HgSO₄ (2.3)=HgCl₂ (2.4)>HgO (3.7)
415 >Hg(NO₃)₂ (12.6).

416 Huang et al. (2013) compared field data collected using the Tekran® system and the
417 UNR active system. Cation-exchange membranes measured concentrations were 1.1-to-3.7 times
418 greater than the nylon membranes, and 2-to-6 times greater than Tekran® RM values.
419 Substantial spatial and temporal variability in the difference between the cation-exchange
420 membrane and Tekran® RM values were observed. Thermal desorption profiles from the nylon
421 membranes indicate this is explained by variability in the Hg(II) compounds present in air
422 (Huang et al., 2013; 2015).

423 Data collected using the UNR Active System can be compared to KCl-coated denuder
424 measurements in different areas and used for understanding the GOM concentrations and
425 chemistry for different areas.

426

427 **4. Case study demonstrating how we can use past measurements to move forward**

428 In light of the new information about interferences affecting GOM measurements, we
429 may begin to go back and re-examine features of past data that previously could not be
430 explained. Here we explore Weiss-Penzias et al. (2003) as a case study. They measured GEM,
431 GOM, and PBM at Cheeka Peak Observatory, Washington, US, in the marine boundary layer
432 and found “air of continental origin containing anthropogenic pollutants contained on average
433 5.3% lower GEM levels as compared with the marine boundary”. GOM and PBM concentrations

434 in continental air were very low, 0 – 20 pg m⁻³ and 1-4 pg m⁻³, respectively. At the time, the
435 results were “difficult to reconcile”. Now we see that the change in GEM concentration during
436 local anthropogenic pollution events relative to the mean of monthly marine air (-60 to -270 pg
437 m⁻³) in Weiss-Penzias et al. (2003) are similar to the disparity in concentrations measured during
438 RAMIX between the DOHGS and Tekran® RM measurement.

439 Retrospectively, we suggest the observed differences between the two air masses reported
440 can be explained by differences in the mix of oxidants and the resultant Hg(II) compounds
441 formed. GOM and PBM were likely low due to lack of collection efficiency, interferences with
442 O₃, and loss in the sampling line (see SI for details of sampling set up). Significantly lower GEM
443 concentrations in the continental air are indicative of greater oxidation, which is supported by
444 decreases in GEM concentrations coincident with O₃ increases. Eastern Washington is covered
445 by forests, which generate volatile organic compounds that could contribute to O₃ and GOM
446 formation. The marine air masses likely contained HgBr₂ or HgCl₂ and the continental air Hg-O,
447 Hg-S, Hg-N compounds associated with industry, agriculture, and mobile sources. The capture
448 efficiency of HgBr₂ and HgCl₂ is greater than for O, S, and N compounds (Figure 1; Table 2).
449 The case study exemplifies how we can use the loss of GEM as a means of understanding the
450 amount of GOM present or produced in air.

451

452 **5. Advancing understanding using Hg measurements and models**

453 Here we discuss several key scientific advancements that have come from comparing
454 models with speciated measurements, as well as the major questions left open by these studies.
455 The number of atmospheric models capable of simulating speciated Hg has multiplied over the
456 last decade (Table 3). Detailed discussion on model/measurement comparisons of RM can be

457 found in Kos et al. (2013). Limitations and uncertainties of the models themselves have been
458 written about at length in original research articles on model intercomparisons (Bullock et al.,
459 2008; Pongprueksa et al., 2008; Lin et al., 2006). Fully acknowledging current limitations, there
460 have still been huge strides made in our scientific understanding of the processes controlling
461 GEM, GOM, and PBM cycling in the atmosphere including: marine boundary layer cycling,
462 plume chemistry, source-receptor relationships, gas-particle partitioning, and vertical
463 distribution.

464 Our understanding of speciated Hg cycling in the marine boundary layer (MBL) is one
465 example of Hg science advancing as a result of using measurements and models in combination.
466 GOM in the MBL has a diurnal pattern characterized by a midday peak and is depleted through
467 deposition at night (Laurier & Mason, 2007; Laurier et al., 2003; Sprovieri et al., 2003). The use
468 of observations and models together determined that the MBL has bromine photochemistry, and
469 was not affected by the hydroxyl (OH) radical. This drives the midday photochemical peak in
470 GOM concentrations in the MBL and that scavenging by sea-salt was driving rapid deposition at
471 night (Holmes et al., 2009; Selin et al., 2007; Obrist et al., 2010; Hedgecock and Pirrone, 2001,
472 2004; Hedgecock et al., 2003; Jaffe et al., 2005; Laurier and Masson 2007; Laurier et al., 2003;
473 Sprovieri et al., 2003) .

474 Model-observation comparisons consistently suggest models overestimate GOM surface
475 concentrations, sometimes by as much as an order of magnitude (Amos et al., 2012; Zhang et al.,
476 2012; Kos et al., 2013; Holloway et al., 2012; Bieser et al., 2014). The measurement-model
477 mismatch is now understood as being partly explained by a low sampling bias (see Section 3),
478 but this alone cannot reconcile the discrepancy. Reduction of GOM to GEM in coal-fired power
479 plant plumes (Edgerton et al., 2006; Lohman et al., 2006) has been invoked as a possible

480 explanation (Amos et al., 2012; Zhang et al., 2012; Kos et al., 2013; Holloway et al., 2012;
481 Vijayaraghavan et al., 2008). The mechanism for in-plume reduction (IPR) remains speculative,
482 hindering inference about how in-plume reduction may vary with coal type, control technology,
483 or atmospheric composition. Results from recent field and laboratory data have been mixed,
484 providing evidence for and against IPR (Tong et al., 2014; Landis et al., 2014) (Deeds et al.,
485 2013). The speciation of anthropogenic emission inventories is also being revisited in order to
486 reconcile model-measurement RM mismatches (Wang et al., 2014; Bieser et al., 2014).

487 Improving our understanding of IPR and emission speciation has important implications for the
488 efficacy of domestic regulation such as the US EPA Mercury Air Toxics Standard and for
489 potentially attributing trends in Hg wet deposition over the US (Zhang et al., 2013).

490 Derived source-receptor relationships will also be sensitive to uncertainties in IPR and
491 emission speciation. On the whole, Hg models simulate wet deposition fluxes better than surface
492 GOM concentrations, contributing to the relatively high degree of consensus among source-
493 receptor studies. A comparison of source-receptor studies found models agreed within 10% in
494 terms of the attribution of total wet Hg deposition to a given continental region (e.g., Europe,
495 Asia) (AMAP/UNEP, 2013; Travnikov et al., 2010). Several source-receptor studies have
496 concluded domestic US emissions contribute ~20% to total Hg deposition over the contiguous
497 US (Selin and Jacob, 2008; Corbitt et al., 2011). Zhang et al. (2012) found that including IPR in
498 a model decreased the domestic contribution to wet deposition over the United States from 22 to
499 10%.

500 An additional area of measurement-model study has been gas-particle partitioning of
501 GOM and PBM. Understanding gas-particle partitioning is important because gases and particles
502 are removed from the atmosphere by different physical processes. There is observational and

503 laboratory evidence that gas-particle partitioning between GOM and PBM is driven by air
504 temperature and aerosol concentrations (Rutter and Schauer, 2007a and b; Steffen et al., 2014)
505 (Rutter et al., 2008; Amos et al., 2012; Chen et al., 2014). Implementing temperature-dependent
506 gas-particle partitioning in a global model increased simulated annual Hg deposition at higher
507 latitudes (Amos et al., 2012). Aircraft observations suggest gas-particle partitioning also plays a
508 major role in influencing the vertical profile of Hg, especially in the upper troposphere/lower
509 stratosphere (UTLS) (Swartzendruber et al., 2009; Lyman and Jaffe, 2012; Murphy et al., 2006).
510 Current gas-particle partitioning relationships are derived from surface data. PBM measurements
511 from the summit of Mt. Bachelor suggest these relationships do not capture PBM dynamics aloft
512 (Timonen et al., 2013). Effects of aerosol composition (Rutter and Schauer, 2007b), relative
513 humidity, or even repartitioning of RM within the Tekran® (see section 3.3) could potentially
514 contribute to this deficiency.

515 Oxidation also plays a central role in Hg cycling at the upper troposphere/lower
516 stratosphere boundary. Comparisons against vertical aircraft profiles of TGM consistently
517 suggest there is too little oxidation in models in the lower stratosphere (Zhang et al., 2012;
518 Holmes et al., 2010). Observations show that total Hg is depleted in the lower stratosphere
519 (Holmes et al., 2010; Lyman and Jaffe, 2012; Slemr et al., 2014), which is thought to be the
520 result of rapid oxidation of Hg(0) to Hg(II), partitioning of Hg(II) to sulfate aerosol, and
521 subsequent sedimentation of PBM (Lyman and Jaffe, 2012). Aircraft measurements over
522 Washington and Tennessee, US, found summertime GOM peaks between 2-4 km
523 (Swartzendruber et al., 2009; Brooks et al., 2014). Modeled GOM vertical profiles over the US
524 have a less pronounced peak and generally place it higher (4-6 km) (Bullock et al., 2008).

525 Correctly modeling the vertical distribution of Hg, particularly GOM and PBM, is essential for
526 simulating deposition and hence Hg loading to surface ecosystems.

527 Chemistry remains one of the greatest uncertainties in Hg models. Improving
528 measurements to determine the chemistry can help determine the mechanism(s) at play. There is
529 still a general lack of rate coefficients and corresponding step-by-step reaction mechanisms
530 available. The estimated tropospheric lifetime of RM against deposition and reduction is 40 days
531 (Holmes et al., 2010), but the reduction pathway is highly uncertain (Subir et al., 2011;
532 Pongprueska et al., 2008), and the burden of RM in the free troposphere is uncertain by at least a
533 factor of two (Selin et al., 2008; De Simone et al., 2014). Improving our knowledge of the
534 reduction and oxidation rates in the atmosphere will allow models to better capture the vertical
535 distribution of Hg, and in turn better simulate Hg deposition. The recent AMAP/UNEP (2013)
536 assessment identified this as the highest priority for Hg models due to the importance in the Hg
537 exposure pathway.

538 A persistent issue is the ambiguity in comparing modeled Hg(II) compounds to GOM and
539 PBM, which are operationally defined. Models either have a lumped Hg(II) tracer or explicitly
540 resolve individual Hg(II) compounds (Table 3). Since different Hg(II) compounds have different
541 collection efficiencies by the KCl-denuder (Figure 1), this further confounds how to best
542 construct a GOM-like model quantity to compare against observations. An active dialogue
543 between experimentalists and modelers is encouraged as the community moves forward, so
544 modelers may implement Hg tracers that emulate the Hg compounds measured.
545 Recent papers have used a 3-fold correction factor to adjust the GOM concentrations measured
546 by the Tekran® system to calculate dry deposition using models in the Western United States
547 and Florida (cf. Huang and Gustin, 2015a; Huang et al. 2015). Use of this correction factor is

548 based on the discrepancy between denuder measurements in the field and cation exchange
549 membranes dry deposition measurements and concentrations collected using the UNR active
550 system. Weiss-Penzias et al. (2015) found the GEOS-Chem model overestimated RM/GEM by a
551 factor of 2.8 compared to Tekran® RM/GEM, which is roughly in line with this correction
552 factor. These field observations were collected in dry and humid conditions, and at O₃
553 concentrations typically observed in the atmosphere. Additional consideration could be based on
554 the RH and O₃ concentrations, and the potential GOM compounds in the air.

555 **6. Outstanding issues**

556 Mercury is present in the atmosphere at pg m⁻³ to ng m⁻³, and the capability to measure it
557 is a substantial analytical accomplishment. Ongoing measurements of atmospheric Hg will be
558 key in evaluating the environmental benefit of regulation on behalf of the Minimata Convention.

559 Here we reviewed the current state of the science for measuring and modeling
560 atmospheric Hg concentrations. Recent laboratory and field investigations have shown numerous
561 artifacts and environmental interferences can affect measurement methods. Some environments
562 such as those with low humidity and O₃ may be less susceptible to sampling interferences than
563 others. In light of new information about the limitations of sampling methods, we may revisit
564 and better explain certain features of previous data sets and measurement-model comparison.

565 Fundamental research is needed on measurement methods and the atmospheric chemistry
566 of Hg. We need to obtain agreement between several methods for understanding the chemical
567 forms and compounds in the air. Only through comparison of multiple calibrated measurements
568 can results be determined to be accurate.

569 Identifying the chemical compounds of RM in the atmosphere is a top priority.
570 Understanding the final oxidation products are key for resolving questions regarding Hg

571 chemistry. Knowing the dominant compounds would help with the design of measurement
572 methods and determination of deposition velocities. Thermal desorption shows promise and mass
573 spectrometry may be a way to verify compounds.

574 Development of a standard, field-deployable calibration system is needed. This system
575 should provide spikes into ambient air and allow for studying sampling efficiencies and artifacts
576 associated with ambient air. Lack of calibration is currently a major shortcoming.

577 A pyrolyzer should be used at the inlet of the 2537 if the goal is to measure TAM. The
578 way the Tekran® 1130/1135 system is configured to capture GOM first and then PBM is the best
579 method to measure these two compounds. However, given the difficulty of separating GOM
580 from PBM, we recommend interpreting the sum of RM instead of PBM alone until separation is
581 improved.

582 A measurement system that collects GOM on a denuder material that has been
583 demonstrated to work for all compounds of GOM, and separate measurement on a filter using a
584 cation-exchange membrane could be used for measurement of GOM and RM. Then PBM could
585 be determined by difference. Due to negative artifacts during long sampling times measurements
586 should be done for < 24 h.

587 A new passive sampler design is needed that quantitatively determines concentrations
588 and is calibrated. Use of a computational fluid dynamics model to help design the sampler could
589 be one successful way forward. Passive samplers and surrogate surfaces have longer time
590 resolution (1 day to 1 week), but are relatively inexpensive and easy to operate and could provide
591 an alternative measure of GOM concentrations and dry deposition fluxes in large-scale sampling
592 networks once the above issues are resolved.

593

594 **Acknowledgements**

595 This manuscript was initiated by discussions at the “Data Collection, Analysis and
596 Application of Speciated Atmospheric Mercury” Workshop coordinated by Leiming Zhang and
597 held 29 July 2014 in San Francisco, California. Work at UNR was supported by the National
598 Science Foundation (Awards: 0850545, 0917934, 1102336, 1326074), the Electric Power
599 Research Institute, and The Southern Company. We thank Drs. Dan Jaffe and Steve Lindberg for
600 comments on an early version of this manuscript. We thank Dr. Franz Slemr for his extensive
601 review and constructive comments, and two anonymous reviewers for their comments; and Tony
602 Hynes for providing information on his instrument that has now been included in the paper.
603 M.S.G. thanks all the undergraduate students who clean glassware, and process and analyze
604 samples in the lab, for this work could not have been done without their conscientious efforts,
605 and Michael Gustin for his continued support.

606

607 **References cited.**

608

609 Aas, W (ed.): Data quality 2004, quality assurance, and field comparisons, C587 EMEP/CCC-Report
610 4/2006, NILU, Kjeller, Norway 2006.

611

612 AMAP/UNEP: Technical Background Report for the Global Mercury Assessment 2013., Arctic Monitoring
613 and Assessment Program, Oslo, Norway / UNEP Chemicals Branch, Geneva, Switzerland, vi + 263 pp,
614 <http://www.unep.org/PDF/PressReleases/GlobalMercuryAssessment2013.pdf> 2013.

615

616 Ambrose, J.L., Lyman, S.N., Huang, J., Gustin, M., Jaffe, D.A.: Fast Time Resolution Oxidized
617 Mercury Measurements with the UW Detector for Oxidized Hg Species (DOHGS) during the Reno
618 Atmospheric Mercury Intercomparison Experiment, Environ. Sci. Technol., 2013.

619

620 Amos, H. M., Jacob, D. J., Holmes, C. D., Fisher, J. A., Wang, Q., Yantosca, R. M., Corbitt, E. S., Galarneau,
621 E., Rutter, A. P., Gustin, M. S., Steffen, A., Schauer, J. J., Graydon, J. A., St Louis, V. L., Talbot, R. W.,
622 Edgerton, E. S., Zhang, Y., and Sunderland, E. M.: Gas-particle partitioning of atmospheric Hg(II) and its
623 effect on global mercury deposition, Atmos. Chem. Phys., 12, 591-603, doi:10.5194/acp-12-591-2012,
2012.

624

625 Barghigiani, C., Ristori, T., Cortopassi, M.: Air mercury measurement and interference of atmospheric
626 contaminants with gold traps, *Environ. Technol.*, 12, 935-941, 1991.

627

628 Bauer, D., Everhart, S., Remeika, J., Tatum Ernest, C., Hynes, A. J.: Deployment
629 of a Sequential Two-Photon Laser Induced Fluorescence Sensor for the Detection
630 of Gaseous Elemental Mercury at Ambient Levels: Fast, Specific, Ultrasensitive Detection
631 with Parts-Per-Quadrillion Sensitivity, *Atmos. Meas. Tech.*, 7, 4251-4265, 2014
632 doi:10.5194/amt-7-4251-2014.

633

634

635 Bauer, D., Campuzano-Jost, P., Hynes, A.J.: Rapid, ultra-sensitive detection of gas phase elemental
636 mercury under atmospheric conditions using sequential two-photon laser induced fluorescence,
637 *Environ. Monit.*, 4, 339-343, 2002.

638

639 Bauer, D., Swartzendruber, P.C., Hynes, A.J.: Deployment of a compact sequential 2 Photon LIF detection
640 system for gaseous elemental mercury at ambient levels, *Geochimica Et Cosmochimica Acta*, 74, A60-
641 A60, 2010.

642

643 Bieser, J., De Simone, F., Gencarelli, C., Geyer, B., Hedgecock, I., Matthias, V., Travnikov, O., and Weigelt,
644 A.: A diagnostic evaluation of modeled mercury wet depositions in Europe using atmospheric speciated
645 high-resolution observations, *Environ. Sci. Pollut. Res.*, 21, 9995-10012, doi: 10.1007/s11356-014-2863-
646 2, 2014.

647 Brosset, C., Iverfeldt, A.: Interaction of solid gold surfaces with mercury in ambient air, *Water Air Soil
648 Poll.*, 43, 147-168, 1989.

649

650 Brooks, S., Ren, X., Cohen, M., Luke, W., Kelley, P., Artz, R., Hynes, A., Landing, W., and Martos, B.:
651 Airborne Vertical Profiling of Mercury Speciation near Tullahoma, TN, USA, *Atmosphere*, 5, 557-574,
652 2014.

653

654 Brunke, E.-G., Labuschagne, C., Ebinghaus, R., Kock, H. H., Slemr, F.: Gaseous elemental mercury
655 depletion events observed at Cape Point during 2007–2008, : *Atmospheric Chemistry and Physics*, 10,
656 1121-1131, 2010.

657

658 Bullock, O. R., Atkinson, D., Braverman, T., Civerolo, K., Dastoor, A., Davignon, D., Ku, J. Y., Lohman, K.,
659 Myers, T. C., Park, R. J., Seigneur, C., Selin, N. E., Sistla, G., and Vijayaraghavan, K.: The North American
660 Mercury Model Intercomparison Study (NAMMIS): Study description and model-to-model comparisons,
661 *J. Geophys. Res.-Atmos.*, 113, 17, doi: 10.1029/2008jd009803, 2008.

662 Castro, M.S., Moore, C., Sherwell, J., Brooks, S.B.: Dry deposition of gaseous oxidized mercury in
663 Western Maryland, *Sci. Total Environ.*, 417, 232-240, 2012.

664

665 Cole, A.S., Steffen, A.: Trends in long-term gaseous mercury observations in the Arctic and effects of
666 temperature and other atmospheric conditions, *Atmos. Chem. Phys.*, 10, 4661-4672, 2010.

667

668 Cole, A.S., Steffen, A., Eckley, C.S., Narayan, J., Pilote, M., Tordon, R., Graydon, J.A., St Louis, V.L., Xu, X.,
669 Branfireun, B.A.: A Survey of Mercury in Air and Precipitation across Canada: Patterns and Trends,
670 *Atmosphere*, 5(3), 635-668, 2014.

671

672 Corbitt, E. S., Jacob, D. J., Holmes, C. D., Streets, D. G., and Sunderland, E. M.: Global Source-Receptor
673 Relationships for Mercury Deposition Under Present-Day and 2050 Emissions Scenarios, *Environ. Sci.*
674 *Technol.*, 45, 10477-10484, doi: 10.1021/es202496y, 2011.

675 Deeds, D.A., Banic, C.M., Lu, J., Daggupaty, S.: Mercury speciation in a coal-fired power plant plume: An
676 aircraft-based study of emissions from the 3640 MW Nanticoke Generating Station, Ontario, Canada,
677 *Geophys. Research-Atmos.*, 118, 4919-4935, 2013.

678

679 Dibble, T.S., Zelie, M.J., Mao, H.: Thermodynamics of reactions of ClHg and BrHg radicals with
680 atmospherically abundant free radicals, *Atmos. Chem. Phys.*, 12, 10271-10279, 2012.

681

682 Ebinghaus, R., Jennings, S.G., Schroeder, W.H., Berg, T., Donaghy, T., Guentzel, J., et al.: International
683 field intercomparison measurements of atmospheric mercury species at Mace Head, Ireland, *Atmos.*
684 *Environ.*, 33, 3063-3073, 1999.

685

686 Engle, M.A., Tate, M.T., Krabbenhoft, D.P., Kolker, A., Olson, M.L., Edgerton, E.S., et al.: Characterization
687 and cycling of atmospheric mercury along the central US Gulf Coast, *Appl. Geochem.*, 23, 419-437, 2008.

688

689 Engstrom, D.R., Fitzgerald, W.F., Cooke, C.A., Lamborg, C.H., Drevnick, P.E., Swain, E.B., et al.:
690 Atmospheric Hg Emissions from Preindustrial Gold and Silver Extraction in the Americas: A Reevaluation
691 from Lake-Sediment Archives, *Environ. Sci. Technol.*, 48, 6533-6543, 2014.

692

693 EPA Method 1631: <http://water.epa.gov/scitech/methods/cwa/metals/mercury/index.cfm> , accessed:
694 December 27, 2014.

695

696 Fain, X., Moosmuller, H., Obrist, D.: Toward real-time measurement of atmospheric mercury
697 concentrations using cavity ring-down spectroscopy. *Atmospheric Chemistry and Physics* , 10: 2879-
698 2892, 2010.

699

700 Finley, B.D., Jaffe, D.A., Call, K., Lyman, S., Gustin, M.S., Peterson, C., et al.: Development, Testing, And
701 Deployment of an Air Sampling Manifold for Spiking Elemental and Oxidized Mercury During the Reno
702 Atmospheric Mercury Intercomparison Experiment (RAMIX), *Environ. Sci. Technol.*, 47, 7277-7284, 2013.

703

704 Deeds, D.A., Banic, C.M., Lu, J., Daggupaty, S.: Mercury speciation in a coal-fired power plant plume: An
705 aircraft-based study of emissions from the 3640 MW Nanticoke Generating Station, Ontario, Canada,
706 *Geophys. Research-Atmos.*, 118, 4919-4935, 2013.

707

708 Gay, D.A., Schmeltz, D., Prestbo, E., Olson, M., Sharac, T., Tordon, R.: The Atmospheric Mercury
709 Network: measurement and initial examination of an ongoing atmospheric mercury record across North
710 America, *Atmos. Chem. Phys.*, 13, 11339-11349, 2013.

711

712 Gustin, M., Jaffe, D.: Reducing the Uncertainty in Measurement and Understanding of Mercury in the
713 Atmosphere, *Environ. Sci. Technol.*, 44, 2222-2227, 2010.

714

715 Gustin, M. S. Exchange of Mercury between the Atmosphere and Terrestrial Ecosystems, in:
716 *Environmental Chemistry and Toxicology of Mercury*, Liu, G., Cai, Y., O'driscoll, N., John Wiley and Sons,
717 Hoboken, New Jersey, 423-452, 2011.

718

719 Gustin, M.S., Huang, J., Miller, M.B., Peterson, C., Jaffe, D.A., Ambrose, J., et al.: Do We Understand
720 What the Mercury Speciation Instruments Are Actually Measuring? Results of RAMIX, *Environ. Sci.*
721 *Technol.*, 47(13), 7295-7306, 2013.

722

723 Gustin, M.S., Lindberg, S.E.: Assessing the contribution of natural sources to the global mercury cycle:
724 The importance of intercomparing dynamic flux measurements, *Fresen. J. Anal. Chem.*, 366, 417-422,
725 2000.

726

727 Gustin, M.S., Lyman, S.N., Kilner, P., Prestbo, E.: Development of a passive sampler for gaseous mercury,
728 *Atmos. Environ.*, 45, 5805-5812, 2011.

729

730 Gustin, M.S., Weiss-Penzias, P.S., Peterson, C.: Investigating sources of gaseous oxidized mercury in dry
731 deposition at three sites across Florida, USA, *Atmos. Chem. Phys.*, 12, 9201-9219, 2012.

732

733 Hedgecock, I. M., and Pirrone, N.: Mercury and photochemistry in the marine boundary layer-modeling
734 studies suggest the in situ production of reactive gas phase mercury, *Atmos. Environ.*, 35, 3055-3062,
735 doi: 10.1016/s1352-2310(01)00109-1, 2001.

736

737 Hedgecock, I. M., Pirrone, N., Sprovieri, F., and Pesenti, E.: Reactive gaseous mercury in the marine
738 boundary layer: modelling and experimental evidence of its formation in the Mediterranean region,
739 *Atmos. Environ.*, 37, S41-S49, doi: 10.1016/s1352-2310(03)00236-x, 2003.

740

741 Hedgecock, I. M., and Pirrone, N.: Chasing quicksilver: Modeling the atmospheric lifetime of Hg-(g)(0) in
742 the marine boundary layer at various latitudes, *Environ. Sci. Technol.*, 38, 69-76, doi:
743 10.1021/es034623z, 2004.

744

745 Holloway, T., Voigt, C., Morton, J., Spak, S. N., Rutter, A. P., and Schauer, J. J.: An assessment of
746 atmospheric mercury in the Community Multiscale Air Quality (CMAQ) model at an urban site and a
747 rural site in the Great Lakes Region of North America, *Atmos. Chem. Phys.*, 12, 7117-7133, doi:
748 10.5194/acp-12-7117-2012, 2012.

749

750 Holmes, C. D., Jacob, D. J., Mason, R. P., and Jaffe, D. A.: Sources and deposition of reactive gaseous
751 mercury in the marine atmosphere, *Atmos. Environ.*, 43, 2278-2285, doi:
752 10.1016/j.atmosenv.2009.01.051, 2009.

753

754 Holmes, C. D., Jacob, D. J., Corbitt, E. S., Mao, J., Yang, X., Talbot, R., Slemr, F.: Global atmospheric model
755 for mercury including oxidation by bromine atoms, *Atmos. Chem. Phys.*, 10, 12037-12057, 2010.

756 Huang, J.Y., Lyman, S.N., Hartman, J.S., Gustin, M.S.: A review of passive sampling systems for ambient
757 air mercury measurements, *Environ. Sci.-Processes & Impacts*, 16, 374-392, 2014.

758

Table captions.

Table 1. Pros and cons of automated and passive methods used to make Hg measurements.

Table 2. Regression equations comparing nylon membrane and cation exchange membrane measured GOM concentrations versus those measured by the denuder using the University of Nevada, Reno (UNR) laboratory manifold system and charcoal scrubbed air.

Table 3. Atmospheric models with speciated mercury .

Figure captions.

Figure 1. Correlation between GOM concentrations measured by KCl-coated denuder versus the nylon and cation exchange membranes in activated charcoal scrubbed air. Modified from Huang et al. (2013).

Figure 2. Thermal desorption profiles generated by permeating different Hg compounds. Modified from Huang et al. (2013). Percent indicates the amount released relative to the total. Profiles were developed in activated charcoal scrubbed air. Compounds being permeated may not be the exact compound in the permeation tube, and this needs to be verified.

Figure 3. Figure 7 from Weiss-Penzias et al. (2003). Reprinted with permission from Weiss-Penzias et al. 2003, Copyright 1 September 2003 American Chemical Society.

Table 1. Pros and cons of automated and integrative methods used to make Hg measurements.

	Hg form measured/detection limit	Pros	Cons	Suggestion/comments
Automated				
Tekran 2537-gold traps	GEM or TGM 0.5 ng m ⁻³ ambient air	Low detection limit, 2.5 to 5 minute resolution, there is a calibration source, standardized by AMNet and CAMNet	Inlet configuration will impact whether measuring GEM or TGM Requires fairly trained technicians, stable	Suggest using a pyrolyzer at the inlet if TAM measurement is desired.

		(cf. Prestbo and Gay, 2009)	electrical source, regular calibration and checks	
Tekran 1130-KCl denuder	GOM 1 pg m ⁻³	Good time resolution (1 to 2 hours)	No calibration source, coating denuders needs to be done by one operator, does not measure all the GOM in air	New method needs to be developed that measures all forms in air and is not impacted by relative humidity and ozone. A different denuder coating would be useful.
Tekran 1135-quartz filter and chips	PBM 1 pg m ⁻³	Good time resolution (1 to 2 hours)	Positive artifact due to measurement of GOM that passes through the denuder, not all PBM is measured due to select grain size capture	Filter method may be best and suggest using cation exchange membranes
Lumex	GEM or TGM in air Total Hg in liquids and solids <1 ng m ⁻³ for air if averaged over 5 minutes	Good time resolution (seconds) Field portable Allows for measurement of Hg concentrations in environmental media in the field	Older version has issues with stability. See SI.	Good for industrial and field applications
Gardias	GEM or TGM 0.5 ng m ⁻³	Good time resolution (2.5 minutes)	Requires trained operators	
DOHGS	GEM and TGM 80 pg m ⁻³	Good time resolution (2.5 minutes)	Requires highly trained operators and stable environment	Useful as a research instrument
Laser	GEM	Fast time resolution	Requires highly trained	Useful as research instrument

		(seconds)	operators and a stable environment,	Could be configured to measure RM and GEM
Manual Active				
GOM Mist Chamber	GOM Blank: 20-50 pg		Complicated operation Need acidified solution	Useful as a research instrument, needs to be re-evaluated
Direct Particulate Matter Sampler Measurement	PBM Probably GOM	Easy operation	Artifacts from GOM partition, choice of filters important to consider as well as length of sampling line and collection time	
UNR Active System	GOM ~30 pg m ⁻³	Easy operation, Useful for quantifying GOM and the chemical forms in air.	Potentially some PBM measured	Good for networks, and it could be used to help calibrate measurements made by the Tekran.
Manual Passive systems				
GEM Passive Sampler	GEM or TGM 10-80 pg m ⁻³	Easy operation	Long time resolution	Good for worldwide network
GOM Passive sampler-concentration	GOM 2.3-5 pg m ⁻³	Easy operation	Long time resolution	Needs a new design
GOM Passive sampler-deposition	GOM Minor PBM 0.02-0.24 pg m ⁻² h ⁻¹	Easy operation Real Hg loading to ecosystem	Long time resolution	Good for worldwide network

Table 2. Regression equations comparing nylon membrane and cation exchange membrane measured GOM concentrations versus those measured by the denuder using the UNR laboratory manifold system and charcoal scrubbed air.

	HgCl ₂	HgBr ₂	HgO	Hg(NO ₃) ₂	HgSO ₄
Nylon membrane (y)	y=1.6x +0.002	y=1.7x +0.01 r ² =0.99, n=10	y=1.8x +0.02 r ² =0.99, n=8	y=1.4x +0.04 r ² =0.90, n=12	y=1.9x -0.1 r ² =0.6, n=12
KCl denuder (x)	n=12				
Cation- exchange membrane (y)	y=2.4x +0.1 r ² =0.58, n=9	y=1.6x+0.2 r ² =0.86, n=5	y=3.7x +0.1 r ² =0.99, n=6	y=12.6x -0.02 r ² =0.50, n=6	y=2.3x +0.01 r ² =0.95, n=18
KCl denuder (x)					

Table 3. Atmospheric models with speciated mercury

Model Name	Domain	Type	Explicit or lumped Hg(II)	References
GRAHM	Global	3D, Eulerian	Explicit (HgCl ₂ , HgO)	Dastoor & Larocque [2004]; Ryaboshopka et al. [2007a,b]; Dastoor et al. [2008]; Durnford et al. [2010]; Kos et al. [2013]; Dastoor et al. [2014]
GEOS-Chem	Global ^a	3D, Eulerian	Bulk Hg(II)	Selin et al. [2008]; Selin & Jacob [2008]; Holmes et al. [2010]; Corbitt et al., [2011]; Amos et al., [2012]; Zhang et al., [2012]; Chen et al. [2014]; Kikuchi et al [2013]
CMAQ-Hg	Continental US	3D, Eulerian	Explicit (HgCl ₂ , HgO)	Bullock & Brehme [2002]; Vijayaraghavan et al. [2008]; Holloway et al. [2012]; Bash et al. [2014]
GLEMOS	Variable, global to regional	3D, Eulerian	Lumped	Travnikov & Ryaboshapko (2002), EMEP report; Travnikov (2010)
ECHMERIT	Global	3D, Eulerian	HgO _(g) , HgCl _{2(g)} , lumped Hg(II) _(aq)	De Simone et al., (2014); Jung et al. (2009)
WRF-Chem	Regional	3D, Eulerian	Lumped	Gencarellia et al 2014
MSCE-Hg- Hem	Northern Hemisphere	3D, Eulerian	HgO _(g) , HgCl _{2(g)} , lumped Hg(II) _(aq)	Travnikov and Ryaboshapko (2002); Travnikov (2005); Travnikov O. and Ilyin I. (2009)
ADOM	North America, Europe	3D, Eulerian	HgO _(g) , HgCl _{2(g)} , lumped Hg(II) _(aq)	Petersen et al. (2001)
DEHM	Northern Hemisphere	3D, Eulerian	HgO _(g) , HgCl _{2(g)} , lumped Hg(II) _(aq)	Christensen et al. (2004); Skov et al. (2004, EST)
WoRM3	Global	2D, Multi- media	Lumped	Qureshi et al. (2011)

PHANTAS	Arctic	Box model	Detailed, explicit Hg(II) compounds	Toyota et al. (2014)
HYSPPLIT	Global	3D, Lagrangian	$\text{HgO}_{(g)}$, $\text{HgCl}_{2(g)}$, lumped $\text{Hg(II)}_{(aq)}$	Cohen et al. 2004
TEAM	North America	3D, Eulerian	$\text{HgO}_{(g)}$, $\text{HgCl}_{2(g)}$, lumped $\text{Hg(II)}_{(aq)}$	Bullock et al. 2008; 2009
CTM-Hg	Global	3D, Eulerian	$\text{HgO}_{(g)}$, $\text{HgCl}_{2(g)}$, lumped $\text{Hg(II)}_{(aq)}$	Shia et al 1999; Seigneur et al. 2001; 2004; 2003; 2006; Lohman et al., 2008
REMSAD	North America	3D, Eulerian	Explicit (HgCl_2 , HgO)	Bullock et al. 2008; 2009
EMAP	Europe	3D, Eulerian	Lumped	Syrakov et al., 1995

^a The standard GEOS-Chem has a global domain with the option to have a nested high-resolution simulation over North America [Zhang et al., 2012]

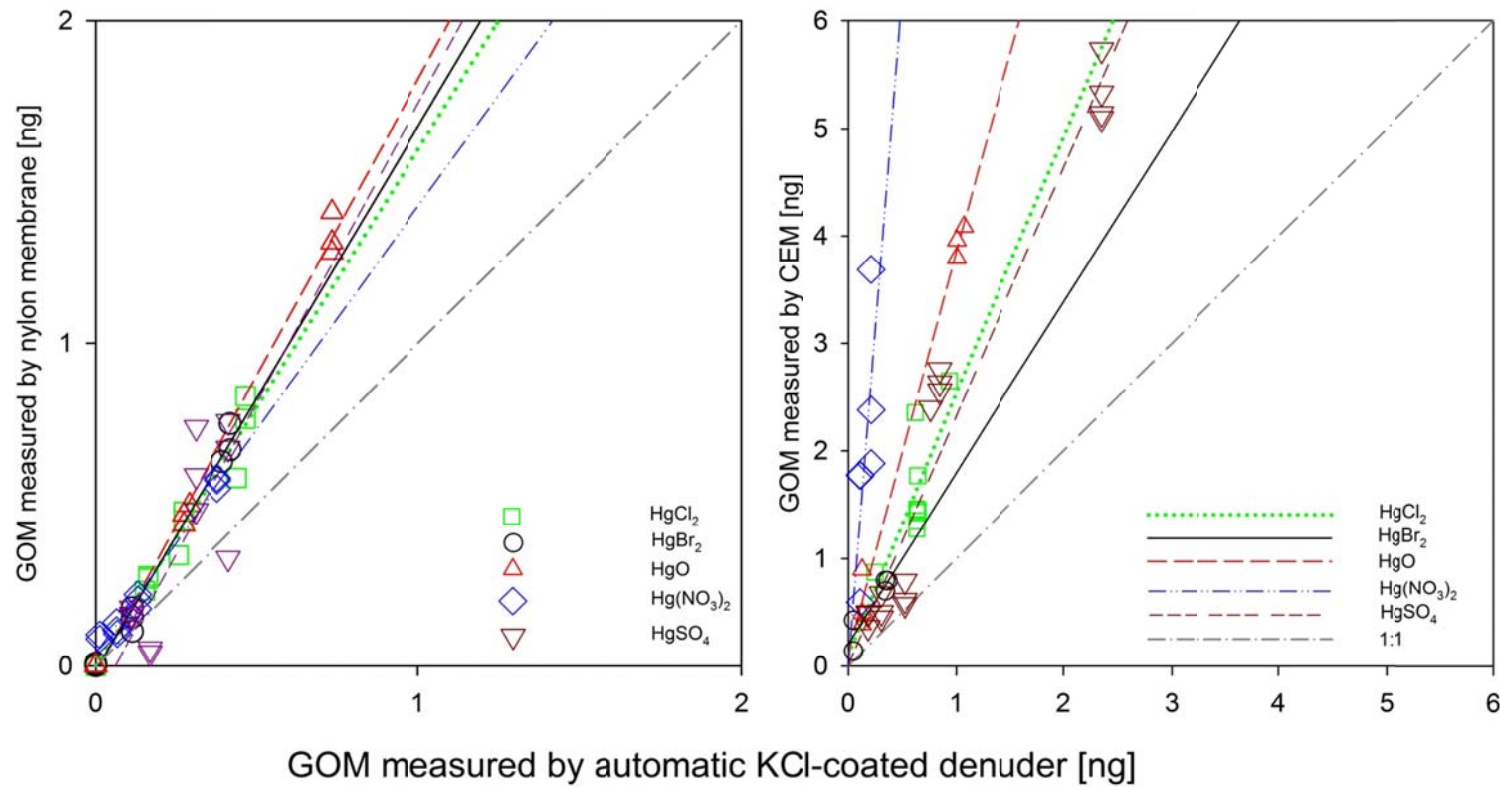


Figure 1. Correlation between GOM concentrations measured by KCl-coated denuder versus the nylon and cation exchange membranes in activated charcoal scrubbed air. Modified from Huang et al. (2013).

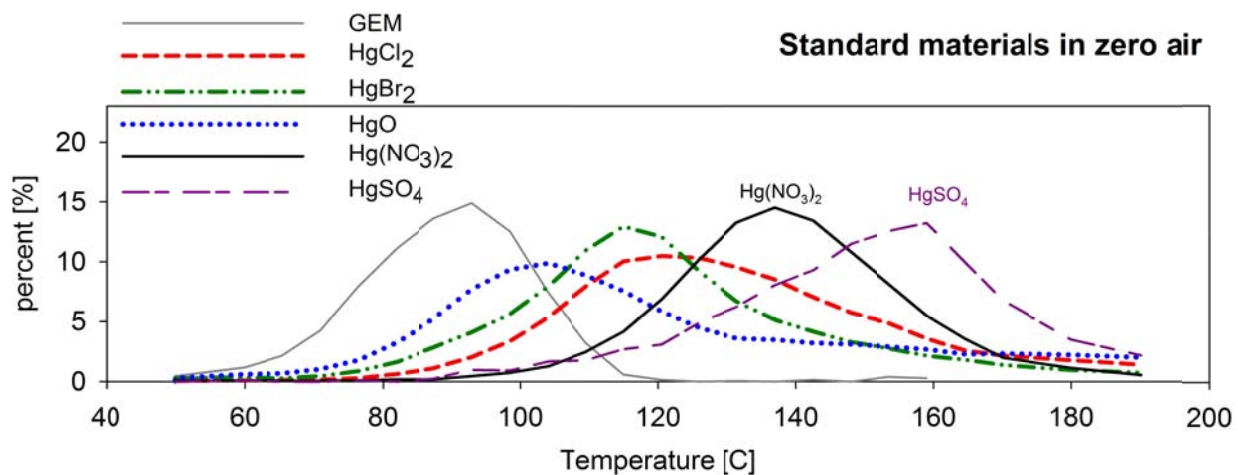


Figure 2. . Thermal desorption profiles generated by permeating different Hg compounds. Modified from Huang et al. (2013). Percent indicates the amount released relative to the total. Profiles were developed in activated charcoal scrubbed air. Compounds being permeated may not be the exact compound in the permeation tube and this needs to be verified.

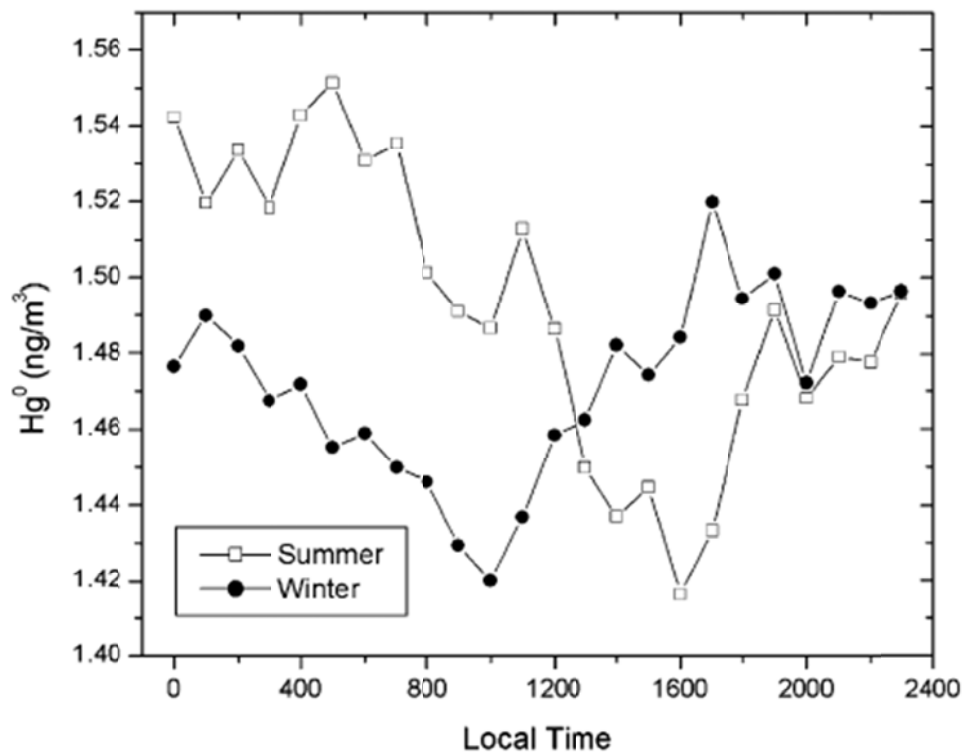


Figure 3. Figure 7 from Weiss-Penzias et al. (2003). Reprinted with permission from Weiss-Penzias et al. 2003, Copyright 1 September 2003 American Chemical Society.